

# Resonance shifts in SPR curves of nonabsorbing, weakly absorbing, and strongly absorbing dielectrics

Sanong Ekgasit<sup>a,b,\*</sup>, Arunchai Tangcharoenbumrungsuk<sup>a</sup>, Fang Yu<sup>b</sup>,  
Akira Baba<sup>b,1</sup>, Wolfgang Knoll<sup>b</sup>

<sup>a</sup> Sensor Research Unit, Department of Chemistry, Faculty of Science, Chulalongkorn University, Bangkok 10330, Thailand

<sup>b</sup> Max-Planck-Institut für Polymerforschung, Ackermannweg 10, D-55128 Mainz, Germany

Received 7 June 2004; accepted 24 July 2004

## Abstract

The resonance shifts (i.e., the resonance angle and the reflectance minimum) in surface plasmon resonance (SPR) curves due to the complex refractive index and/or thickness variations of dielectric films were investigated. For both, nonabsorbing and absorbing dielectrics, the resonance angle shifts linearly with the refractive index and/or thickness variations. The reflectance minimum of the nonabsorbing dielectric does not change as the resonance angle shifts. For an absorbing dielectric, the direction of the reflectance change depends strongly on the magnitude of the absorption and thickness of the metal film. The reflectance minimum of the sensor with a thin metal film decreases before increasing while that of the sensor with a thick metal film continuously increases as the absorption of the dielectric film increases. The phenomena were theoretically explained based on the SPR-generated evanescent field at the metal/dielectric interface associated with the optical properties of the sensor architecture.

© 2004 Elsevier B.V. All rights reserved.

**Keywords:** SPR; Surface plasmon resonance; Evanescent field; Absorbing dielectrics; Nonabsorbing dielectrics

## 1. Introduction

Surface plasmon resonance (SPR) spectroscopy is a surface sensitive characterization technique that takes advantage of the resonance coupling between the exciting radiation and the surface plasmon wave propagates along the surface of a thin noble metal film for probing changes near the metal surface. The resonance coupling of the incident light and the surface plasmon wave can be tailored for specific applications by altering the structure of the metal film or the environment in the vicinity of the metal surface [1–4]. Due to the highly sensitive nature of the surface plasmon wave towards the optical properties of the dielectric media near the metal surface, SPR sensor becomes a powerful affinity biosensor for monitoring interactions at the interface (i.e., enzyme–substrate,

antigen–antibody, receptor–ligand, and drug–protein interactions) or physicochemical phenomena near the metal surface (i.e., chemical reactions, absorption, degradation, swelling, protein hybridizations, and self-assembling). The sensitive nature of the SPR sensor is derived from the unique characteristic of the surface plasmon resonance (SPR)-generated evanescent field at the metal/dielectric interface under the total internal reflection condition. The field is strongest at the metal/dielectric interface due to the resonance coupling. The strong SPR-generated evanescent field decays exponentially as a function of distance into the metal film and the dielectric medium. The rapid decay of the evanescent field makes SPR sensor very sensitive to changes of the optical constant and/or thickness of the dielectric film attached to the metal film. This change can be observed via the shift of the resonance angle of the SPR curve [2–7].

The physicochemical phenomena at the metal surface, especially those associated with binding or interaction of biomolecules at the interface, involve mass accumulation on the sensor surface, which induces refractive index and/or

\* Corresponding author. Tel.: +662 218 7585; fax: +662 218 7598.

E-mail address: [sanong.e@chula.ac.th](mailto:sanong.e@chula.ac.th) (S. Ekgasit).

<sup>1</sup> Present address: Department of Chemistry, University of Houston, 136 Fleming Building, Houston, TX 77204-5003, USA.

thickness variation of the dielectric film. By employing a functionalized dielectric film, specific interaction on the sensor surface can be monitored. The molecular structure–biological function and/or structure–property relationship of the molecules associated with the interaction can be studied. The linear relationship between the SPR signal and the refractive index and/or thickness changes enables SPR for quantitative analysis of the interaction [2–7].

Although SPR sensor has been traditionally employed for monitoring physicochemical phenomena associated with nonabsorbing dielectrics, its sensitivity improvement by absorbing dielectrics has recently gained substantial attentions [8–21]. For a nonabsorbing dielectric film, the resonance angle shifts linearly with the refractive index and/or thickness changes without a significant change of the reflectance minimum. The progress of the interaction at the sensor surface can be derived from the linear shift of the resonance angle or the reflectance change monitored at an angle slightly lower than the resonance angle [2–4]. In the SPR sensitivity improvement scheme via the absorbing dielectric, the combination of resonance angle shift due to refractive index and/or thickness changes and reflectance change due to the additional absorption makes SPR sensor very sensitive when it is used for monitoring the physicochemical phenomena associated with absorbing dielectrics. Gold and silver nanoparticles and gold colloid have been employed for sensitivity enhancement of SPR-based biosensor [8–13]. The enhancement techniques take advantage of the reflectance change due to the high absorption index of the additionally bound nanoparticles. Based on the specific binding scheme, the additionally bound gold nanoparticles enhance the detection limit of binding events, especially those of small molecules such as DNA fragments. In general, the binding of small molecules induces insignificant changes in the SPR curve due to the extremely small refractive index and/or thickness variation [21–22]. The reflectance minimum change due to absorption at a low concentration of bulk dielectric has been employed as a sensitive detection scheme for enzyme-based SPR sensor [15]. The strong SPR-generated evanescent field has also been employed for excitation of the surface-confined fluorophore near the metal surface in surface plasmon field-enhanced fluorescence spectroscopy [17–21].

This paper will show that various unique characteristics and sensitive nature of the SPR technique are governed by the SPR-generated evanescent field at the metal/dielectric interface. The changes of SPR curve associated with complex refractive index and/or thickness variations of the nonabsorbing dielectrics, weakly absorbing dielectric, and strongly absorbing dielectrics are theoretically explained via the SPR-generated evanescent field.

## 2. Theory

For an SPR setup in the Kretschmann–Raether ATR configuration, reflectance depends strongly on the experimental

conditions (i.e., polarization, angle of incidence, and wavelength of the coupled radiation) and material characteristics (i.e., the complex refractive indices of the metal films, the dielectric films and the dielectric substrate, and the thickness of the metal and the dielectric films). Under the total internal reflection condition, the reflectance  $R(\theta)$  of the coupled radiation with parallel polarization can be expressed in terms of the evanescent field amplitude and optical properties of the materials by the following expression [23,24]:

$$R(\theta) = 1 - A(\theta) = 1 - \left(\frac{2\pi}{\lambda}\right)^2 \frac{1}{k_{zP}(\theta)} \sum_{j=1}^N \left[ \int_{z_j}^{z_{j+1}} \text{Im}[\hat{\epsilon}_j] \langle E_z^2(\theta) \rangle dz \right] \quad (1)$$

where  $\theta$  is the angle of incidence,  $A(\theta)$  the absorption in *absorptance unit*,  $\lambda$  the wavelength of the coupled radiation,  $\hat{\epsilon}_j$  the complex dielectric constant of the  $j$ -th layer, and  $\langle E_z^2(\theta) \rangle$  the mean square evanescent electric field at a distance  $z$  from the prism/metal interface.  $N$  is the number of the dielectric film in the sensor architecture with the metal film as the first layer.  $k_{zP}(\theta)$  is the  $z$ -component of the wavevector in the prism.  $k_{zP}(\theta)$  can be expressed in terms of the  $x$ -component of the wavevector  $k_{xP}(\theta)$  by  $k_{zP}(\theta) = [(2\pi/\lambda)^2 \epsilon_P - k_{xP}^2(\theta)]^{1/2}$  with  $k_{xP}(\theta) = (2\pi/\lambda)[\epsilon_P \sin^2 \theta]^{1/2}$  and  $\epsilon_P$  is the dielectric constant of the prism. The complex dielectric constant is related to the complex refractive index by  $\hat{\epsilon} = \hat{n}^2 = (n + ik)^2$ ; where  $n$  and  $k$ , respectively, are refractive index and absorption index. The detailed derivations of the electric field and the reflectance based on the surface SPR-generated evanescent field are given elsewhere [23–25].

For SPR of a nonabsorbing dielectric, the metal film is the only absorbing medium in the sensor architecture. The reflectance can be expressed in terms of the evanescent field within the metal film and the optical property of the metal film by [23,24]:

$$R(\theta) = 1 - \left(\frac{2\pi}{\lambda}\right)^2 \frac{1}{k_{zP}(\theta)} \int_0^{d_M} \text{Im}[\hat{\epsilon}_M] \langle E_z^2(\theta) \rangle dz \quad (2)$$

where  $d_M$  and  $\hat{\epsilon}_M$ , respectively, are thickness and complex dielectric constant of the metal film. Although the nonabsorbing dielectric does not contribute to the reflection loss in the SPR curve, its refractive index and thickness govern the resonance condition of the SPR curve. The resonance angle shifts to a greater value without a significant change in the reflectance minimum as the thickness and/or refractive index of the nonabsorbing dielectric film increase.

The SPR curve of an absorbing dielectric is characterized by a broader curve shape together with a greater reflectance minimum compared to that of the nonabsorbing dielectric. This is due to the presence of an additional absorbing media in the sensor architecture. When an absorbing dielectric presents in the system, smaller evanescent field amplitude at the metal/dielectric interface compared to that of the nonabsorbing dielectric is observed. The reflectance with absorbing

dielectrics can be expressed in terms of the evanescent field by [24]:

$$R(\theta) = 1 - \left(\frac{2\pi}{\lambda}\right)^2 \frac{1}{k_z P(\theta)} \left\{ \int_0^{d_M} \text{Im}[\hat{\epsilon}_M] \langle E_z^2(\theta) \rangle dz + \sum_{l=1}^L \left[ \int_{d_{Dl}} \text{Im}[\hat{\epsilon}_{Dl}] \langle E_z^2(\theta) \rangle dz \right] \right\} \quad (3)$$

where  $d_{Dl}$  and  $\hat{\epsilon}_{Dl}$ , respectively, are thickness and complex dielectric constant of the  $l$ -th dielectric film, while  $\int_{d_{Dl}}$  indicates integration over the thickness of the film.  $l$  is the number of dielectric films.

### 3. Experimental

#### 3.1. SPR setup

A schematic illustration of an SPR setup is shown in Fig. 1. A radiation from a HeNe laser (632.8 or 1152 nm) was modulated by a chopper. The plane of polarization and intensity of the modulated radiation were controlled by two polarizers. The radiation was coupled to the systems via a right-angled prism (LaSFN9 or BK7). The reflected beam was then focused onto a photodiode detector. The SPR signals were collected as a function of the measured incidence angle  $\theta_e$  defined with respect to the direction normal to the prism/metal interface. The measured incidence angle  $\theta_e$  is slightly different from the incident angle  $\theta$  at the prism/metal interface due

to the refraction at the air/prism interface. For direct comparisons with the experimental results, the simulated results were expressed in terms of the measured incidence angle  $\theta_e$  while the calculated reflectance was corrected for the reflection at the prism surfaces.

#### 3.2. Sensor fabrications

Glass wafers (LaSFN9 or BK7) were cleaned and coated with a  $\sim 50$  nm gold film via a thermal evaporation instrument (Edwards FL400, England) at a deposition rate of 0.1 nm/s under UHV condition ( $5 \times 10^{-6}$  mbar). The BK7 wafers were pre-coated with  $\sim 1$  nm chromium adhesion promoter layer prior to the coating of gold film. Freshly gold-coated wafers were employed for all experiments.

##### 3.2.1. Antibody binding experiment (SPR of nonabsorbing and weakly absorbing dielectrics)

The self-assembled monolayer (SAM) was fabricated by immersing the gold-coated LaSFN9 wafers in the thiol solutions over night at room temperature. Ethanol solutions of mixed thiols (OH-terminated thiol and biotin-terminated thiol with a net thiol concentration of 500  $\mu$ M) with mole fractions of the biotin-terminated thiol  $\chi$  of 0.1 and 0.04 were employed. After the SAM fabrication, the substrates were rinsed thoroughly with absolute ethanol, blown-dry with dry nitrogen, and kept under argon environment until being used. The experiments were performed by injecting an aliquot of 1 mL fluorophore-labeled antibody AF-2F5 (Alexa Fluor 647-labeled mouse monoclonal antibody 2F5 (isotype IgG<sub>1,k</sub>) with dye-to-protein ratio of 4.4, Molecular Probes) into the flow cell. The solution was left in the flow cell for 15 min in order to allow the complete binding of the antibody onto the surface of SAM. The sensors were regenerated by flow washing the antibody-bound SAM with a sodium dodecyl sulfate solution (5 mg/mL in HBS-EP). Once the regeneration is completed (i.e., no additional change in the observed SPR curve after prolonged washing), a binding with a non-labeled antibody 2F5 was performed. After the binding of the non-labeled antibody, the final binding with fluorophore-labeled antibody AF-RaM (Alexa Fluor 647-labeled rabbit anti-mouse IgG with dye-to-protein ratio of 4.8, Molecular Probes) was then carried out. All experiments were performed at room temperature ( $21 \pm 2^\circ\text{C}$ ) with HBS-EP buffer solution (degassed 10 mM HEPES-buffered saline, pH 7.4, 150 mM NaCl, 3 mM EDTA with 0.005% (v/v) surfactant P-20, Biacore, Sweden). An equal working concentration of 20 nM was employed for the fluorophore-labeled antibody AF-2F5 and the non-labeled antibody 2F5 while a concentration of 33 nM was employed for the fluorophore-labeled antibody AF-RaM. In order to avoid bulk solution effect, the cell was flow-washed and filled with running buffer before an SPR acquisition. The SPR curves of the step-by-step binding events are shown in Fig. 2.

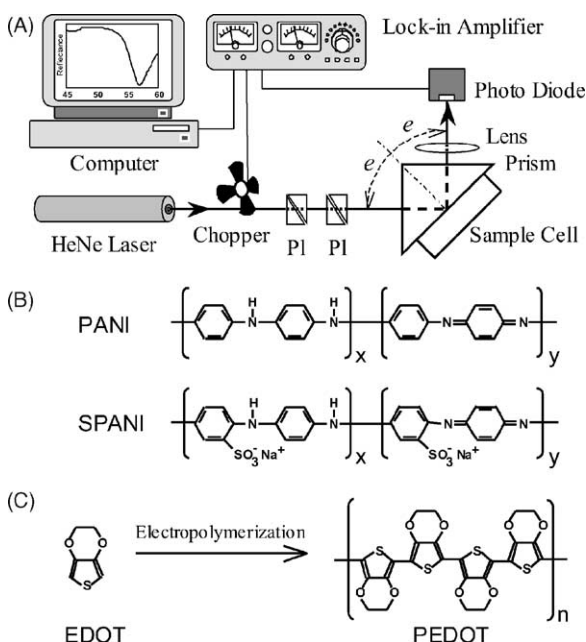


Fig. 1. (A) A schematic illustration of an SPR experimental setup. (B) Structures of polyaniline (PANI) and sulfonated polyaniline (SPANI). (C) Structures of 3,4-ethylenedioxythiophene (EDOT) and poly(3,4-ethylenedioxythiophene) (PEDOT).

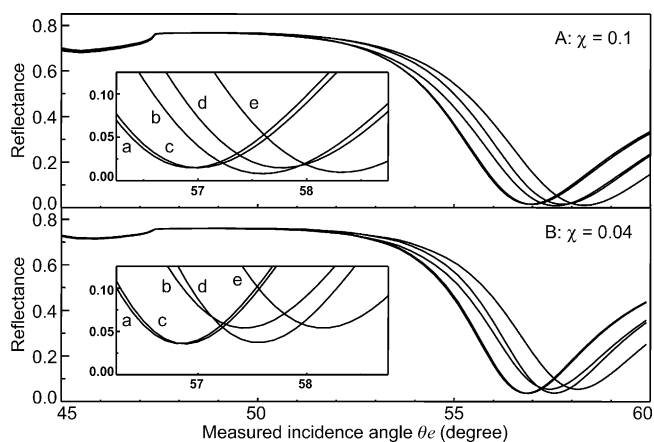


Fig. 2. SPR curves of the binding of antibodies onto the surface of SAM with the mole fraction of biotin-terminated thiol of (A)  $\chi = 0.1$  and (B)  $\chi = 0.04$ . The sensor architectures are: (a) Au/SAM; (b) Au/SAM/AF-2F5; (c) Au/SAM (regenerated); (d) Au/SAM/2F5; and (e) Au/SAM/2F5/AF-RaM. Note: AF-2F5 and AF-RaM are fluorophore-labeled antibodies (weakly absorbing dielectrics).

### 3.2.2. Self-assembled conducting polymer experiment (SPR of a strongly absorbing dielectric with thickness variation)

The gold-coated BK7 wafer was functionalized by immersing in the solution of 3-mercaptopropylsulfonic acid, sodium salt (0.001 M in ethanol). The uniform and negatively charged substrate was immersed in a dilute HCl solution prior to the self-assembled fabrications. The substrates were alternatively immersed, for 15 min, in aqueous solution of the polycation and the polyanion until the desired numbers of self-assembled layers were achieved (i.e., 2, 4, and 6 layers) [26]. The fabricated wafer was rinsed thoroughly with deionized water (Milli-Q, 18 M $\Omega$ , pH 5.6) between the successive depositions. Structures of the polyelectrolyte are shown in Fig. 1. Polyaniline (PANI) and sulfonated polyaniline (SPANI) were synthesized following the procedures given by MacDiarmid et al. [27] and Yue et al. [28], respectively. Poly(allylamine hydrochloride) (PAH; MW 50,000–65,000) and poly(sodium 4-styrenesulfonate) (PSS; MW 70,000) were purchased from Aldrich. The synthesized emeraldine hydrochloride was converted to emeraldine base by reacting with ammonium hydroxide for 24 h. The polymer can be made water soluble according to a procedure given by Cheung et al. [29]. A dilute solution of the polymer (20 mg/mL in dimethylacetamide) was subsequently diluted (1:10) in water (pH 3.0–3.3). The pH of the aqueous solution was then adjusted to approximately pH 2.6. Sulfonation of PANI was performed by reacting with fuming sulfuric acid and isolating the product, which is soluble in 0.1 M sodium hydroxide. The pH of the SPANI solution was adjusted to approximately pH 3.0 prior to self-assembled fabrication [30]. The SPR curves of the multilayer PANI/SPANI films under ambient air environment are shown in Fig. 3.

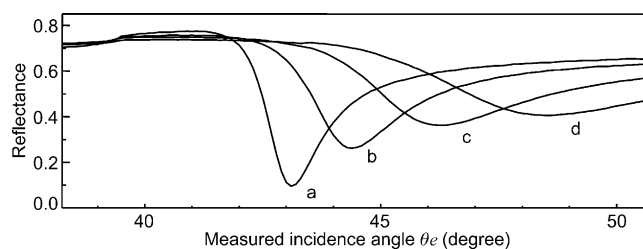


Fig. 3. SPR curves of self-assembled PANI/SPANI conducting polymer films with air as an ambient substrate: (a) Au; (b) Au/(PANI/SPANI); (c) Au/(PANI/SPANI) $\times 2$ ; (d) Au/(PANI/SPANI) $\times 3$ .

### 3.2.3. PEDOT film under applied potential experiment (SPR of strongly absorbing dielectrics with complex refractive index variation)

The ultra thin PEDOT, poly(3,4-ethylenedioxythiophene), film was electropolymerized from a 0.01 M of EDOT monomer (3,4-ethylenedioxythiophene) in acetonitrile with 0.1 M TBAPF6 (tetrabutylammonium hexafluorophosphate) on the surface of a gold-coated LaSFN9 wafer at an applied potential of 0.9 V for 30 s [31]. A conventional three-electrode cell was employed (i.e., the gold-coated LaSFN9 working electrode, a platinum wire counter electrode, and an Ag/Ag<sup>+</sup> non-aqueous reference electrode). The ultra thin PEDOT film was then subjected to different applied potentials via a potentiostat (Princeton Applied Research 263A, EG&G) under a monomer-free solution of 0.1 M TBAPF6 in acetonitrile. The SPR curves with the coupled wavelengths of 632.8 and 1152 nm were acquired after applying a desired potential for 2.5 min. The SPR curves of the ultra thin PEDOT film with the applied potentials of 0.5,  $-0.2$ ,  $-0.65$ , and  $-1.0$  V are shown in Fig. 4.

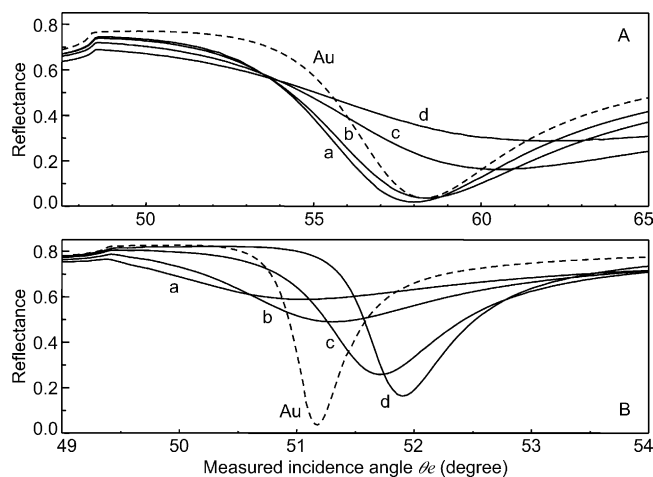


Fig. 4. SPR curves of ultra thin electropolymerized PEDOT at the coupled wavelengths of (A) 632.8 nm and (B) 1152 nm at various applied potentials: (a) +0.50; (b)  $-0.20$ ; (c)  $-0.65$ ; and (d)  $-1.00$  V. SPR curves of the bare gold film under the monomer-free solution of 0.1 M TBAPF6 in acetonitrile are shown (dotted lines).

#### 4. Results

The SPR curves of nonabsorbing and weakly absorbing dielectrics with mole fractions of the biotin-terminated thiol  $\chi$  of 0.10 and 0.04 are shown in Fig. 2A and 2B, respectively. The broad SPR curve in Fig. 2A(a) compared to that in Fig. 2B(a) indicates a thinner gold film. When a weakly absorbing dielectric, the fluorophore-labeled antibody AF-2F5, was bound onto the surface of SAM with  $\chi = 0.10$ , the resonance angle shifted to a greater angle while the reflectance minimum slightly decreased, Fig. 2A(b). The SPR curve retreated back and almost superimposed with that of the virgin SAM when the fluorophore-labeled antibody was removed by the regeneration process, Fig. 2A(c). When a nonabsorbing dielectric, the non-labeled antibody 2F5, was bound onto the regenerated surface, the resonance angle shifted to a greater angle without a significant change of the reflectance minimum, Fig. 2A(d). The magnitude of the shift is slightly greater than that of the fluorophore-labeled antibody. When the fluorophore-labeled antibody AF-RaM was additionally bound onto the sensor, the resonance angle shifted further with a slight decrease of the reflectance minimum, Fig. 2A(d).

Similar resonance angle shifts were observed when the same binding events were performed on the sensor with  $\chi = 0.04$ , Fig. 2B. The change in the reflectance minimum was not observed after the binding of the non-labeled antibody, Fig. 2B(d). However, the increments of the reflectance minimum were detected after the binding of the fluorophore-labeled antibodies, Fig. 2B(b) and (e).

For SPR of a strongly absorbing dielectric, the influences of the absorption via thickness increment were clearly observed in the SPR curves of the self-assembled PANI/SPANI conducting polymer film, Fig. 3. The resonance angle shifted to a greater value, the reflectance minimum increased, the SPR curve became broader while the resonance angle and the critical angle were less obvious as the number of the self-assembled PANI/SPANI film increased. The largest reflectance increment was observed when the first layer of PANI/SPANI film was fabricated onto the gold surface. Smaller increments were detected with the successive self-assembled layers.

The influence of the absorption by the complex refractive index variations was examined via the SPR curves of PEDOT conducting polymer films under various applied potentials,

Table 1  
Fitting parameter of the observed SPR Curves in Fig. 2

| SPR curve  | Layer architecture of the sensor <sup>a</sup>                     |                      |   |                               | $\theta_{\text{eSPR}}^{\text{b}}$ |
|------------|---|----------------------|---|-------------------------------|-----------------------------------|
|            | Au  | SAM                  | AF-2F5 <sup>c</sup> or 2F5                | AF-RaM <sup>d</sup>           |                                   |
|            | Complex refractive index ( $\hat{n} = n + ik$ )<br>Thickness (nm) |                      |   |                               |                                   |
| Fig. 2A(a) | <b>0.139 + i3.607</b><br>42.00                                    | <b>1.500</b><br>1.60 |   |                               | 56.9°                             |
| Fig. 2A(b) | <b>0.139 + i3.607</b><br>42.00                                    | <b>1.500</b><br>1.60 | <b>1.450 + i0.019<sup>c</sup></b><br>5.00 |                               | 57.6°                             |
| Fig. 2A(c) | <b>0.139 + i3.607</b><br>42.00                                    | <b>1.500</b><br>1.60 |   |                               | 56.9°                             |
| Fig. 2A(d) | <b>0.139 + i3.607</b><br>42.00                                    | <b>1.500</b><br>1.60 | <b>1.450</b><br>6.32                      |                               | 57.8°                             |
| Fig. 2A(e) | <b>0.139 + i3.607</b><br>42.00                                    | <b>1.500</b><br>1.60 | <b>1.450</b><br>6.32                      | <b>1.450 + i0.017</b><br>4.40 | 58.3°                             |
| Fig. 2B(a) | <b>0.198 + i3.580</b><br>51.00                                    | <b>1.500</b><br>1.40 |   |                               | 56.9°                             |
| Fig. 2B(b) | <b>0.198 + i3.580</b><br>51.00                                    | <b>1.500</b><br>1.40 | <b>1.450 + i0.034<sup>c</sup></b><br>4.05 |                               | 57.4°                             |
| Fig. 2B(c) | <b>0.198 + i3.580</b><br>51.00                                    | <b>1.500</b><br>1.40 |   |                               | 56.9°                             |
| Fig. 2B(d) | <b>0.198 + i3.580</b><br>51.00                                    | <b>1.500</b><br>1.40 | <b>1.450</b><br>5.15                      |                               | 57.6°                             |
| Fig. 2B(e) | <b>0.198 + i3.580</b><br>51.00                                    | <b>1.500</b><br>1.40 | <b>1.450</b><br>5.15                      | <b>1.450 + i0.032</b><br>4.33 | 58.2°                             |

The values of the complex refractive indices are represented by bold characters.

<sup>a</sup> An LASFN9 Glass ( $n = 1.845$ ) is employed as a coupling prism while the HBS-EP buffer (1.333) is employed as a semi-infinitely thick nonabsorbing ambient substrate.

<sup>b</sup> The measured angle of incidence  $\theta_{\text{e}}$  has a resolution of 0.1° near the resonance angle.

<sup>c</sup> Alexa Fluor 647-labeled mouse monoclonal antibody 2F5 (isotype IgG<sub>1,k</sub>).

<sup>d</sup> Alexa Fluor 647-labeled rabbit anti-mouse IgG.

Table 2  
Fitting parameter of the observed SPR Curves in Fig. 3

| SPR curve | Layer architecture of the sensor <sup>a</sup>   |                              |                             |                             |                             | $\theta_{\text{eSPR}}^{\text{b}}$ |
|-----------|---|------------------------------|-----------------------------|-----------------------------|-----------------------------|-----------------------------------|
|           | Cr <sup>c</sup>                                 | Au                           | PANI/SPANI                  | PANI/SPANI                  | PANI/SPANI                  |                                   |
|           | Complex refractive index ( $\hat{n} = n + ik$ ) |                              |                             |                             |                             |                                   |
|           | Thickness (nm)                                  |                              |                             |                             |                             |                                   |
| Fig. 3a   | <b>3.66 + i4.36</b><br>0.70                     | <b>0.20 + i3.48</b><br>55.30 |                             |                             |                             | 43.1°                             |
| Fig. 3b   | <b>3.66 + i4.36</b><br>0.70                     | <b>0.20 + i3.48</b><br>55.30 | <b>1.50 + i0.22</b><br>6.00 |                             |                             | 44.4°                             |
| Fig. 3c   | <b>3.66 + i4.36</b><br>0.70                     | <b>0.20 + i3.48</b><br>55.30 | <b>1.50 + i0.22</b><br>6.00 | <b>1.50 + i0.22</b><br>7.40 |                             | 46.3°                             |
| Fig. 3d   | <b>3.66 + i4.36</b><br>0.70                     | <b>0.20 + i3.48</b><br>55.30 | <b>1.50 + i0.22</b><br>6.00 | <b>1.50 + i0.22</b><br>7.40 | <b>1.50 + i0.22</b><br>7.20 | 48.5°                             |

The values of the complex refractive indices are represented by bold characters.

<sup>a</sup> A BK7 Glass ( $n = 1.515$ ) is employed as a coupling prism while air ( $n = 1.00$ ) is employed as a semi-infinitely thick nonabsorbing ambient substrate.

<sup>b</sup> The measured angle of incidence  $\theta_e$  has a resolution of  $0.1^\circ$  near the resonance angle.

<sup>c</sup> The complex refractive index is obtained from reference [34].

Fig. 4. The SPR curve of the bare gold with 0.1 M TABPF6 solution at the coupled wavelength of 1152 nm, Fig. 4B, was narrower than that with the coupled wavelength of 632.8 nm. At the coupled wavelength of 632.8 nm, Fig. 4A, the resonance angle and the reflectance minimum of the SPR curve

with the 0.5 V applied potential were smaller than those with negatively applied potentials. When the film was subjected to a negatively applied potential (i.e.,  $-0.2$ ,  $-0.65$ , and  $-1.0$  V), the reflectance minimum increased while the resonance angle shifted to greater value and became less obvious.

Table 3  
Fitting parameter of the observed SPR curves in Fig. 4

| SPR curve  | Layer architecture of the sensor <sup>a</sup>   |                                | $\theta_{\text{eSPR}}^{\text{b}}$ |
|------------|---|--------------------------------|-----------------------------------|
|            | Au  | PEDOT                          |                                   |
|            | Complex refractive index ( $\hat{n} = n + ik$ ) |                                |                                   |
|            | Thickness (nm)                                  |                                |                                   |
| Fig. 4A(a) | <b>0.198 + i3.569</b><br>40.00                  |                                | 58.3°                             |
| Fig. 4A(b) | <b>0.198 + i3.569</b><br>40.00                  | <b>1.328 + i0.049</b><br>22.50 | 58.0°                             |
| Fig. 4A(c) | <b>0.198 + i3.569</b><br>40.00                  | <b>1.343 + i0.067</b><br>22.10 | 58.5°                             |
| Fig. 4A(d) | <b>0.198 + i3.569</b><br>40.00                  | <b>1.404 + i0.178</b><br>21.30 | 60.4°                             |
| Fig. 4A(e) | <b>0.198 + i3.569</b><br>40.00                  | <b>1.406 + i0.341</b><br>19.70 | 61.9°                             |
| Fig. 4B(a) | <b>0.230 + i8.066</b><br>40.00                  |                                | 51.2°                             |
| Fig. 4B(b) | <b>0.230 + i8.066</b><br>40.00                  | <b>1.230 + i0.239</b><br>22.50 | 51.1°                             |
| Fig. 4B(c) | <b>0.230 + i8.066</b><br>40.00                  | <b>1.322 + i0.170</b><br>22.10 | 51.3°                             |
| Fig. 4B(d) | <b>0.230 + i8.066</b><br>40.00                  | <b>1.445 + i0.083</b><br>21.30 | 51.7°                             |
| Fig. 4B(e) | <b>0.230 + i8.066</b><br>40.00                  | <b>1.514 + i0.026</b><br>19.70 | 51.7°                             |

The values of the complex refractive indices are represented by bold characters.

<sup>a</sup> An LASFN9 Glass ( $n = 1.845$ ) is employed as a coupling prism while the 0.1 M TBAPF6 in acetonitrile ( $n = 1.340$ ) is employed as a semi-infinitely thick nonabsorbing ambient substrate.

<sup>b</sup> The measured angle of incidence  $\theta_e$  has a resolution of  $0.1^\circ$  near the resonance angle.

With the same potentials applied on the exact same PE-DOT film, opposite phenomena were observed with the coupled wavelength of 1152 nm. The broadest SPR curve with the highest reflectance minimum and the smallest resonance angle was observed at the 0.5 V applied potential. The resonance angle shifted to a greater value while the reflectance minimum decreased as the film was subjected to a greater negatively applied potential (i.e.,  $-0.2$ ,  $-0.65$ , and  $-1.0$  V, respectively).

In order to determine the layer architectures and to gain insight understandings of the investigated systems, the observed SPR curves were fitted by Fresnel equation. The fitted parameters are shown in Tables 1–3.

## 5. Discussion

For binding events of nonabsorbing dielectrics, the resonance angle increases without a significant change of the reflectance minimum (i.e., Fig. 2A(c) and (d) and Fig. 2B(c) and (d)). This phenomenon associates with the evanescent field in the metal film. The evanescent field at the resonance angle does not change significantly as it shifts to a greater angle by the deposition of a nonabsorbing dielectric. Fig. 5A shows the resonance shift (i.e., the resonance angle and the reflectance minimum) of the SPR curve induced by thickness and refractive index increments. The resonance angle shifts linearly with thickness and refractive index of the nonabsorbing film. The reflectance minimum, however, stays unchanged.

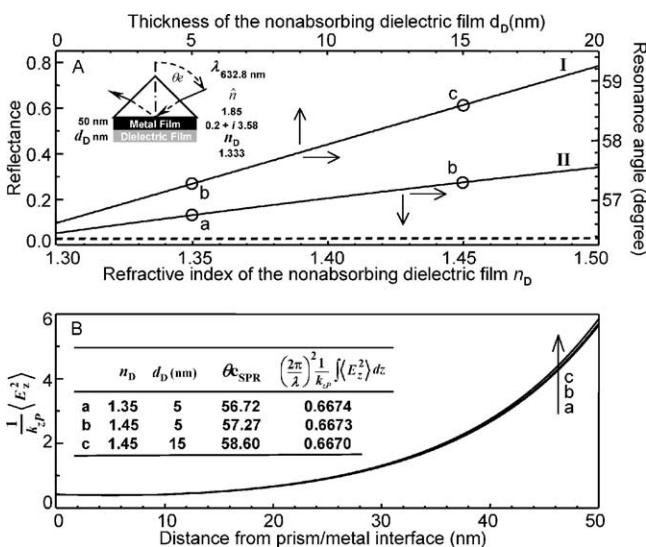


Fig. 5. (A) The resonance condition of a nonabsorbing dielectric film: (I) thickness variation of a film with  $n_D = 1.45$ ; (II) refractive index variation for a film with  $d_D = 5$  nm thick. The solid lines indicate the resonance angle while the dotted lines (two lines are superimposed) indicate the reflectance minimum. (B) The evanescent field decay profile within the metal film at three different conditions: a, b, and c, defined in (A). The insert shows the evanescent field integrations at the resonance angles. The layer architecture of the system and the coupled wavelength are shown in the figure. Note: the positions labeled-(b) have the same layer architecture.

the metal film is the only absorbing medium in the SPR of the nonabsorbing dielectrics, the attenuation of the reflectance can be assigned to the absorption of the metal.[23,24] According to Eq. (2), the reflectance is proportional to the integration of the product between the evanescent field amplitude and the imaginary part of the dielectric constant of the metal film, the evanescent field integration must be constant or insignificantly changed as the resonance angle shifts. Fig. 5B shows the evanescent field decay profile at three different resonance conditions defined in Fig. 5A. Although their resonance angles are different, the corresponding evanescent field decay profiles within the metal film are almost the same. The same magnitudes of the evanescent field integrations make their reflectance minimums almost the same (i.e., cannot be differentiated experimentally, see Fig. 5A).

SPR of an absorbing dielectric is more complicated than that of the nonabsorbing dielectric due to the presence of an additional absorbing medium. The resonance angle shifts to a greater angle due to the thickness and/or refractive index increment. The reflectance minimum also changes while the SPR curve becomes broader as the absorption of the absorbing dielectric increases. The direction of the reflectance change (i.e., increasing or decreasing) depends strongly on the thickness of the metal film. For a weakly absorbing dielectric, if the thickness of the metal film is smaller than the optimal thickness, the reflectance minimum decreases as the absorption of the dielectric film increases (see Fig. 2A). The opposite phenomenon is observed when the thickness of the metal film is greater than the optimal thickness (see Fig. 2B).

The optimal thickness of the metal film in SPR measurement depends strongly on the wavelength of the coupled radiation and optical constants of the metal film and the dielectric medium. As shown in Fig. 6, the optimal thickness of the gold film decreases as the absorption of the dielectric film increases. For a weakly absorbing thin dielectric film, the optimal gold thickness can be estimated from that of the nonabsorbing dielectric since their evanescent field profiles are not significantly different. Based on the complex dielectric constant from Fresnel fitting, the optimal thickness of the gold film in Fig. 2A is 45.56 nm while that in Fig. 2B is 45.40 nm. The calculated optimal thickness, thus, confirms that the gold film in Fig. 2A is thinner than optimal thickness.

The evanescent field decay profiles at the resonance angles of the SPR curves in Fig. 2 are shown in Fig. 7. The weaker evanescent field in the system with absorbing dielectric makes the absorption of the gold film smaller than that of the gold film in the system with nonabsorbing dielectric. For the system with a thin gold film, Fig. 2A, the decreased absorption of gold film can be compensated by the absorption of the fluorophore-labeled antibody. The summation of the absorption of the gold film and that of the fluorophore-labeled antibody (i.e., Fig. 2A(b) and (e)) is greater than that of the gold film with unbound SAM or with non-labeled antibody (i.e., Fig. 2A(a) and (d)). As a result, according to Eq.

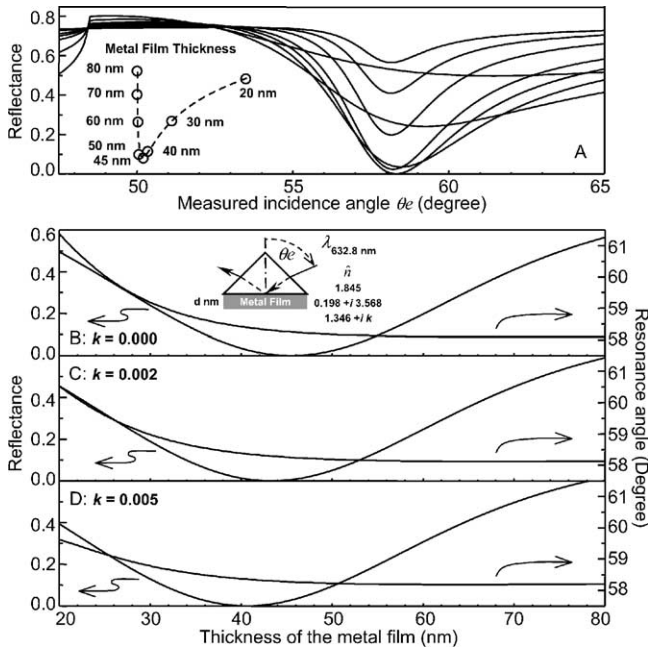


Fig. 6. (A) SPR curves at various metal film thickness. The resonance conditions (resonance angle and reflectance minimum) at various absorption indices  $k$  of the bulk absorbing dielectric with  $\hat{n} = 1.346 + ik$ : (B)  $k = 0.000$ ; (C)  $k = 0.002$ ; and (D)  $k = 0.005$ . The simulation parameters are shown. Note: the resonance conditions in (B) are those of the SPR curves in (A).

(3), smaller reflectance minimums in SPR curves of absorbing dielectric compared to that of the nonabsorbing dielectric are observed. If the absorption of the dielectric film is greatly increased, the evanescent field is significantly decreased. The absorption of the dielectric will not compensate absorption of the metal film, thus, a greater reflectance minimum compared to that of the nonabsorbing dielectric will be observed. The opposite phenomena are observed in the system with a thick gold film. As shown in Fig. 7, the evanescent field is significantly decreased as the dielectric film becomes absorbing. The absorption of the dielectric film cannot com-

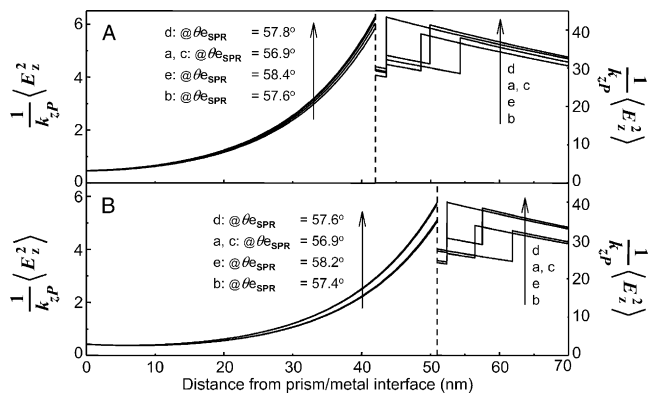


Fig. 7. The evanescent field decay profiles at the resonance angles of the SPR curves: (A) in Fig. 2A and (B) in Fig. 2B. The dotted lines indicate the metal/dielectric interfaces. The simulation parameters are shown in Table 1. The curve labels are associated with those of Fig. 2.

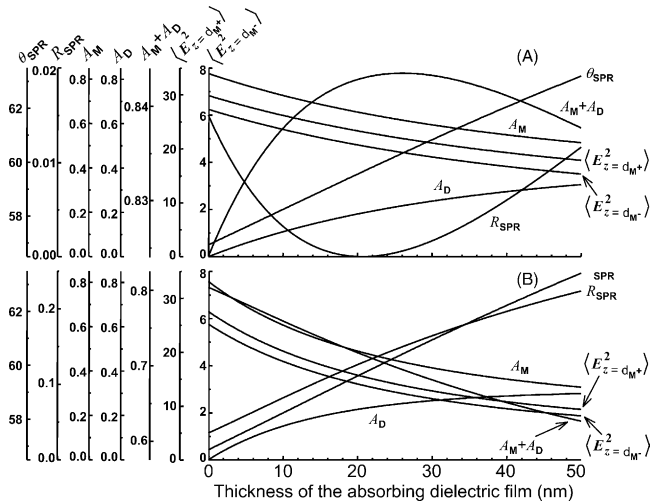


Fig. 8. Parameters at the resonance condition as the thickness of the absorbing dielectric film increases (i.e., via thickness increment) for sensors with thickness of the gold film (A) thinner than the optimal thickness and (B) thicker than the optimal thickness. The simulation parameters are shown in Table 1 (i.e., fitting parameters of Fig. 2A(b) and B(b), respectively) with an increasing thickness of AF-2F5 layer. The y-axes are parameters at the resonance condition ( $\theta_{SPR}$ , resonance angle;  $R_{SPR}$ , reflectance minimum;  $A_M$ , absorptance of the metal film;  $A_D$ , absorptance of the absorbing dielectric;  $A_M + A_D$ , the total absorptance;  $\langle E_z^2 = d_{M+} \rangle$ , evanescent field at the metal/dielectric interface on the metal side and  $\langle E_z^2 = d_M \rangle$ , that on the dielectric side).

pensate the decreased absorption of gold, thus, a greater reflectance is observed (Fig. 2B(b) and (e)).

The changes associated with the increased absorption of the dielectric film via the thickness increment, as summarized in Fig. 8, include: the resonance angle linearly shifts to a greater value, the evanescent field at the metal/dielectric interface decreases, the absorption of the metal film decreases while the absorption of the absorbing dielectric increases. However, the change of the reflectance minimum depends strongly on the thickness of the gold film. For a sensor with a gold film thinner than the optimal thickness, Fig. 8A, the reflectance minimum decreases to a minimal value (almost zero) before continuously increasing as the thickness of the dielectric film increases. This is due to the associated absorptions of the gold film and the absorbing dielectric film. The absorption of a thin dielectric film (i.e., less than 20 nm in this case) is greater than the decreased absorption of the metal film. Thus, the total absorption increases with the thickness of the dielectric film. The high absorption of the dielectric film is due to the strong evanescent field at the metal/dielectric interface. Although, the absorption index and thickness of the dielectric film are much smaller than those of the metal film, the evanescent field in the dielectric medium is much greater than that in the metal film. According to the employed sensor architecture, the evanescent field at the metal/dielectric interface on the dielectric side is 30 times greater than that of the coupled radiation. The evanescent field at the metal/dielectric interface on the metal side, on the other hand, is only six times greater (see Fig. 8). As the thickness of the absorbing dielec-

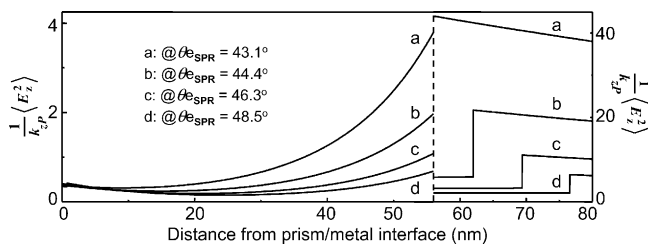


Fig. 9. The evanescent field decay profiles at the resonance angles of the SPR curves in Fig. 3. The simulation parameters are shown in Table 2. The curve labels are associated with those of Fig. 3.

tric film is further increased, the SPR-generated evanescent field is further decreased. Although the absorption of the dielectric film increases, the increased absorption cannot compensate the decreased absorption of the metal film. As a result, the total absorption decreases as the thickness of the metal film increases. According to Eq. (3), this results in a greater reflectance minimum compared to that of the nonabsorbing dielectric film.

For a sensor with a thick gold film, Fig. 8B, the reflectance minimum increases with the thickness of the absorbing dielectric film. The evanescent field decreases as the absorption of the dielectric film increases. The absorption of the metal film, then, decreases due to the weaker evanescent field. Although the absorption of the dielectric film increases with the thickness of the dielectric film, the increased absorption cannot compensate the decreased absorption of the metal film. As a result, the reflectance minimum of the absorbing dielectric is greater than that of the nonabsorbing dielectric.

The broader SPR curve with high reflectance minimum in the SPR curve of a strongly absorbing self-assembled PANI/SPANI film is due to the very weak evanescent field associated with the absorption of the dielectric. The increased absorption of the dielectric film due to thickness increment cannot compensate the decreased absorption of the metal film. As shown in Fig. 9, a substantial decrement of the evanescent field is observed at the first deposition of the self-assembled PANI/SPANI while smaller decrements are observed in the consecutive depositions. As a result, the largest reflectance change is observed upon the deposition of the first layer. Beside the decreased evanescent field amplitude at the metal/dielectric interface, the difference between the absorption maximum of the metal film and that of the dielectric is a contributing factor to the broadening of the SPR curve. [23].

When the physicochemical phenomenon induces a significant change in the complex refractive index of the dielectric film attached to the gold surface, the corresponding SPR curve changes substantially. The refractive index and/or thickness variation shifts the resonance angle while the absorption index change alters the minimum reflectance. The smaller resonance angle in Fig. 4A(a) and B(a) compared to that of the bare gold implies that the refractive index of the PEDOT film with 0.5 V applied potential is smaller than that of the ambient solution (0.1 M TBAPF6 in acetonitrile). Although the thickness variations of the PEDOT film in Fig. 4

were very small, as confirmed by the quartz crystal microbalance (QCM) measurement [31], substantial SPR curve variations caused by the complex refractive index changes were clearly observed. The thickness changes of the conducting polymer films upon applied potential were also reported elsewhere. [32,33] The greater reflectance minimums and the broader SPR curves compared to that of the bare gold film indicate absorptions of the PEDOT film at the coupled wavelengths. The broad SPR curve of bare gold in Fig. 4A (Au) indicates that the 40 nm gold thickness is smaller than the optimal value at 632.8 nm excitation wavelength. According to the dielectric constant of the gold film obtained from the Fresnel fitting, the optimal gold thickness equals 45.48 nm. The above statement is confirmed by the SPR curve with 0.5 V applied potential where the reflectance minimum is smaller than that of the bare gold film. Although the film is weakly absorbing at 0.5 V applied potential, it becomes highly absorbing under the negatively applied potentials. Thus, the reflectance minimum becomes greater than that of the bare gold film as the absorption increases. The observation in Fig. 4A confirms the prediction shown in Fig. 8A.

According to the results from Fresnel fitting, the optimal thickness of the gold film at 1152 nm is 40.48 nm. Despite the slightly smaller film thickness compared to the optimal thickness, the greater absorption index of the gold at 1152 nm makes the SPR curves narrower than that at 632.8 nm. The SPR curve at 0.5 V applied potential indicates that the PEDOT film is strongly absorbing at 1152 nm. In contrast to those at 632.8 nm, PEDOT film becomes less absorbing under the negatively applied potential. The phenomenon predicted in Fig. 8A is not observed in Fig. 4B due to the strong absorption of the PEDOT film and a slightly smaller thickness of the gold film compared to the optimal thickness at the coupled wavelength of 1152 nm (i.e., 40.00 nm compared to 40.48 nm).

## 6. Conclusions

The resonance condition of an SPR curve is greatly influenced by the experimental parameters and optical properties of the materials involving in the sensing scheme. The physicochemical phenomena induce changes in the optical properties of the dielectric film attached to the metal film thus shift the resonance condition. The resonance angle shifts linearly with the refractive index and/or thickness variations. The reflectance minimum change, on the other hand, depends strongly on the absorption of the dielectric film and thickness of the metal film. For a nonabsorbing dielectric, the resonance angle shifts without a significant change in the reflectance minimum. For a sensor with a thin metal film, the reflectance minimum decreases before continuously increases as the absorption of the dielectric film increases. The reflectance minimum of the sensor with a thick metal film, on the other hand, continuously increases as the absorption of the absorbing dielectric increases.

## Acknowledgments

S.E. gratefully acknowledges supports from the Thailand Research Fund (TRF Contract Number RSA/07/2545) and the Alexander von Humboldt (AvH) Foundation.

## References

- [1] W.L. Barnes, A. Dereux, T.W. Ebbesen, Surface plasmon subwavelength optics, *Nature* 424 (2003) 824–830.
- [2] W. Knoll, Interfaces and thin films as seen by bound electromagnetic waves, *Annu. Rev. Phys. Chem.* 49 (1998) 569–638.
- [3] J. Homola, S.S. Yee, G. Gauglitz, Surface plasmon resonance sensors: review, *Sens. Actuators B, Chem.* 54 (1999) 3–15.
- [4] Z. Salamon, H.A. Macleod, G. Tollin, Surface plasmon resonance spectroscopy as a tool for investigating the biochemical and biophysical properties of membrane protein systems 1 theoretical principles, *Biochim. Biophys. Acta* 1331 (1997) 117–129.
- [5] J. Homola, Present and future of surface plasmon resonance biosensors, *Anal. Bioanal. Chem.* 377 (2003) 528–539.
- [6] R.J. Green, R.A. Frazier, K.M. Shakesheff, M.C. Davies, C.J. Roberts, S.J.B. Tendler, Surface plasmon resonance analysis of dynamic biological interactions with biomaterials, *Biomaterials* 21 (2000) 1823–1835.
- [7] M.A. Cooper, Label-free screening of bio-molecular interactions, *Anal. Bioanal. Chem.* 377 (2003) 834–842.
- [8] L.A. Lyon, D.J. Pena, M.J. Natan, Surface plasmon resonance of Au colloid-modified Au films: particle size dependence, *J. Phys. Chem. B* 103 (1999) 5826–5831.
- [9] E. Hutter, J.H. Fendler, D. Roy, Surface plasmon resonance studies of gold and silver nanoparticles linked to gold and silver substrates by 2-aminoethanethiol and 1,6-hexanedithiol, *J. Phys. Chem. B* 105 (2001) 11159–11168.
- [10] T. Okamoto, I. Yamaguchi, Optical absorption study of the surface plasmon resonance in gold nanoparticles immobilized onto a gold substrate by self-assembly technique, *J. Phys. Chem. B* 107 (2003) 10321–10324.
- [11] L. He, M.D. Musick, S.R. Nicewarner, F.G. Salinas, S.J. Benkovic, M.J. Natan, C.D. Keating, Colloidal Au-enhanced surface plasmon resonance for ultrasensitive detection of DNA hybridization, *J. Am. Chem. Soc.* 122 (2000) 9071–9077.
- [12] W. Fritzsche, T.A. Taton, Metal nanoparticles as labels for heterogeneous, chip-based DNA detection, *Nanotechnology* 14 (2003) R63–R73.
- [13] T. Liu, J. Tang, L. Jiang, The enhancement effect of gold nanoparticles as a surface modifier on DNA sensor sensitivity, *Biochem. Biophys. Res. Commun.* 313 (2004) 3–7.
- [14] A. Hanning, J. Roeraade, J.J. Delrow, R.C. Jorgenson, Enhanced sensitivity of wavelength modulated surface plasmon resonance devices using dispersion from a dye solution, *Sens. Actuators B* 54 (1999) 25–36.
- [15] K. Kurihara, K. Nakamura, E. Hirayama, K. Suzuki, An absorption-based surface plasmon resonance sensor applied to sodium ion sensing based on an ion-selective optode membrane, *Anal. Chem.* 74 (2002) 6323–6333.
- [16] T. Wakamatsu, T. Nakano, K. Shinbo, K. Kata, F. Kaneko, Detection of surface-plasmon evanescent fields using a metallic probe tip covered with fluorescence, *Rev. Sci. Instrum.* 70 (1999) 3962–3966.
- [17] T. Liebermann, W. Knoll, P. Sluka, R. Herrmann, Complement hybridization from solution to surface-attached probe-oligonucleotides observed by surface-plasmon field-enhanced fluorescence spectroscopy, *Colloids Surf. A* 169 (2000) 337–350.
- [18] T. Liebermann, W. Knoll, Surface-plasmon field-enhanced fluorescence spectroscopy, *Colloids Surf. A* 171 (2000) 115–130.
- [19] R. Roy, J. Kim, J.T. Kellis, A.J. Poulouse Jr., C.R. Robertson, A.P. Gast, Surface plasmon resonance/surface plasmon enhanced fluorescence: an optical technique for the detection of multicomponent macromolecular adsorption at the solid/liquid interface, *Langmuir* 18 (2002) 6319–6323.
- [20] F. Yu, D.F. Yao, W. Knoll, Surface plasmon field-enhanced fluorescence spectroscopy studies of the interaction between an antibody and its surface-coupled antigen, *Anal. Chem.* 75 (2003) 2610–2617.
- [21] T. Neumann, M.L. Johansson, D. Kambhampati, W. Knoll, Surface-plasmon fluorescence spectroscopy, *Adv. Funct. Mater.* 12 (2002) 575–586.
- [22] J. Spinke, M. Liley, H.-J. Guder, L. Angermaier, W. Knoll, Molecular recognition at self-assembled monolayers—the construction of multicomponent multilayers, *Langmuir* 9 (1993) 1821–1825.
- [23] S. Ekgasit, C. Thammacharoen, W. Knoll, Surface plasmon resonance spectroscopy based on evanescent field treatment, *Anal. Chem.* 76 (2004) 561–568.
- [24] S. Ekgasit, C. Thammacharoen, F. Yu, W. Knoll, Evanescent field in surface plasmon resonance and surface-plasmon field-enhanced fluorescence spectroscopies, *Anal. Chem.* 75 (2004) 2210–2219.
- [25] W.N. Hansen, Electric fields produced by propagation of plane coherent electromagnetic radiation in a stratified medium, *J. Opt. Soc. Am.* 58 (1968) 380–390.
- [26] A. Baba, M.-K. Park, R.C. Advincula, W. Knoll, Simultaneous surface plasmon optical and electrochemical investigation of layer-by-layer self-assembled conducting ultrathin polymer films, *Langmuir* 18 (2002) 4648–4652.
- [27] A.G. MacDiarmid, J.C. Chiang, A.F. Richter, N.L.D. Somasiri, A.J. Epstein, L., in: Alcacer (Ed.), *Conducting Polymers*, Reidel, Dordrecht, 1985, pp. 105–120.
- [28] J. Yue, A.J. Epstein, Synthesis of self-doped conducting polyaniline, *J. Am. Chem. Soc.* 112 (1990) 2800–2801.
- [29] J.H. Cheung, W.B. Stockton, M.F. Rubner, Molecular-level processing of conjugated polymers. 3. Layer-by-layer manipulation of polyaniline via electrostatic interactions, *Macromolecules* 30 (1997) 2712–2716.
- [30] A. Baba, J. Lübber, K. Tamada, W. Knoll, Optical properties of ultrathin poly(3,4-ethylenedioxythiophene) films at several doping levels studied by in situ electrochemical surface plasmon resonance spectroscopy, *Langmuir* 19 (2003) 9058–9064.
- [31] M. Ferreira, M.F. Rubner, M. F. Molecular-level processing of conjugated polymers. 1. Layer-by-layer manipulation of conjugated polyions, *Macromolecules* 28 (1995) 7107–7114.
- [32] N.S. Murthy, L.W. Shacklette, R.H. Baughmann, Effect of charge-transfer on chain dimension in transpolyacetylene, *J. Chem. Phys.* 87 (1987) 2346–2348.
- [33] N.J. Winokur, P. Walmsley, J. Moulton, P. Smith, A.J. Heeger, Structural evolution in iodine-doped poly(3-alkylthiophenes), *Macromolecules* 24 (1991) 3812–3815.
- [34] D. Roy, Surface plasmon resonance spectroscopy of dielectric coated gold and silver film on supporting metal layers: reflectivity formulas in the Kretschmann formalism, *Appl. Spectrosc.* 55 (2001) 1046–1052.